THAI NGUYEN UNIVERSITY
UNIVERSITY OF AGRICULTURE AND FORESTRY

NGUYEN THUY GIANG

STUDY ON THE ANTIBIOTIC TREATMENT IN WATER USING PHOTOCATALYTIC TECHNOLOGY BASED ON DOPED g-C_3N_4 MATERIALS

Major: Environmental Science
Code: 9.44.03.01

SUMMARY OF DOCTORAL DISSERTATION
IN ENVIRONMENTAL SCIENCE

THAI NGUYEN – 2025

The doctoral dissertation was completed at:
UNIVERSITY OF AGRICULTURE AND FORESTRY - THAI NGUYEN UNIVERSTITY

Scientific supervisors: 1. Prof. Dr. Nguyen The Hung

2. Assoc. Prof. Dr. Dang Van Thanh

Reviewer 1:

Reviewer 2:

Reviewer 3:

The dissertation was defended in front of
the institutional dissertation evaluation Committee
Meeting at: University of Agriculture and Forestry
– Thai Nguyen Universtity
On ....., day ..... month .... year 2025

The dissertation can be found at:
- National Library
- Thai Nguyen Learning Resource Center;
- Library of University of Agriculture and Forestry - Thai Nguyen University.

THE LIST OF PUBLISHED WORKS RELATED TO THE DISSERTATION

1. Thuy Giang Nguyen, Manh Dung Nguyen*, Thi Lan Do*, Van Thanh Dang, Thanh-Binh Nguyen, Vu Hoang Huong, 2024. Efficient photocatalytic degradation of sulfamethoxazole in water using in situ synthesized porous tubular boron-doped graphitic carbon nitride. **Surfaces and Interfaces**, vol. 54, 105009. Online: 01/09/2024. SCIE/Q1/IF: 5,7. https://doi.org/10.1016/j.surfin.2024.105009

2. Nguyen Thuy Giang, Nguyen Duy Hai, Phan Dinh Quang, Vu Hoang Huong, Nguyen Viet Hung, Nguyen Manh Dung***,** 2024. The visible light-driven activation of peroxymonosulfate for boosting tetracycline degradation using B-doped g-C_3N_4 nanotubes. **Science and Technology Development Journal**, vol. 26 (S2), 10-19. Published: 30/06/2024. https://doi.org/10.32508/stdj.v26iS2.4271.

3. Nguyen Thuy Giang, Do Thi Lan, Nguyen Manh Dung, 2024. Nghiên cứu chế tạo vật liệu Mo pha tạp g-C_3N_4 trong xử lí ô nhiễm dư lượng kháng sinh trong nước. **Kỷ yếu Hội thảo khoa học quốc gia** "Môi trường nông nghiệp, nông thôn và Phát triển bền vững", Học viện nông nghiệp .

INTRODUCTION

1.1. Research motivation

In recent years, the use of antibiotics in the medical and agricultural sectors has led to antibiotic residue in the water environment, causing many serious problems such as drug resistance, water pollution, and impacts on human health and the ecosystem.

Photocatalytic technology, especially the use of doped g-C_3N_4 (GCN) materials, has shown potential in effectively treating antibiotic residues. This research aims to develop and optimize the process of using doped g-C_3N_4 to remove antibiotic residues in water, thereby minimizing negative impacts on the environment and public health.

Therefore, the thesis topic: "**Study on the antibiotic treatment in water using photocatalytic technology based on doped g-C_3N_4 materials**" is conducted to meet the urgent need for environmental protection, address water pollution caused by antibiotic residues, and contribute to the protection of the ecosystem as well as clean water sources for the community.

1.2. New findings of the dissertation

- The dissertation successfully synthesized porous tubular boron-doped g-C_3N_4 nanomaterials using environmentally friendly methods such as hydrothermal and calcination techniques. Specifically, 1DBCN has a uniform tubular structure with dimensions of 3 x 300 nm, specific surface area of 81.1 m^2/g and band gap energy of 2.7 eV, while TGCN-Bx has a more diverse structure with specific surface area ranging from 85 to 98 m^2/g, the band gap energies of TGCN-Bx (x = 1, 2, 3, 4) are estimated to be 2.7, 2.68, 2.66, 2.64 and 2.61 eV, respectively.The resulting material exhibits uniform porous tubular structures, high specific surface area, and excellent visible-light absorption capacity. These properties significantly enhance photocatalytic activity, particularly in degrading organic pollutants such as antibiotic residues in water.

- The porous tubular boron-doped g-C_3N_4 nanomaterial achieved up to 99% removal efficiency of antibiotic residues under laboratory-scale photocatalytic conditions. A noteworthy aspect of

this study is the comprehensive evaluation of various operational parameters influencing the degradation performance, including reaction time, pollutant concentration, catalyst dosage, pH range (3–11), and the presence of common anions and cations typically found in real wastewater. Simulating realistic environmental conditions enabled the identification of optimal parameters for the potential application of the material in treating antibiotic-contaminated wastewater.

Chapter 1. LITERATURE REVIEW

1.1. Water pollutants, transmission routes, and toxicity

In the past few decades, antibiotic residues in water have become a serious global issue, especially with the increasing use of antibiotics in medicine and agriculture. The main sources of antibiotic residues are raw or treated wastewater from urban areas, hospitals, and wastewater treatment plants, as well as from sewer leaks and surface runoff in urban or agricultural areas (Wu và cs., 2022). In Vietnam, the use of veterinary antibiotics was estimated at 2,751 tons in 2015, mainly for pig farming (58%), aquaculture (31%), and poultry (7%). Several Southeast Asian countries such as Indonesia, Myanmar, and the Philippines are projected to significantly increase the use of antibiotics for food animals in the coming years (150% to 200% from 2010 to 2030) (Carrique-Mas và cs., 2020).

1.2. Overview of antibiotic pollution

Antibiotics can harm the ecosystem, reduce biodiversity, and cause antibiotic resistance in microorganisms. Wastewater from hospitals, pharmaceutical manufacturing plants, and livestock farms are the main sources of water pollution by antibiotic residues. The detection and treatment of antibiotic residues are important for protecting public health and the environment. Treatment technologies such as electrochemical oxidation, adsorption, membrane technology, ultrasonic irradiation, ion exchange, electrolysis, and biological reactions have been studied to remove antibiotic residues. However, the high energy consumption in these processes makes them costly and unsustainable (Kamilya, 2022).

1.3. Wastewater treatment technologies for antibiotics

In recent years, advanced oxidation processes have become the optimal technology for treating wastewater containing polluting organic compounds (Ghime và Prabir Ghosh, 2020). GCN, a metal-free and environmentally friendly semiconductor, has attracted significant attention in science and technology. Although GCN has many advantages such as a suitable band gap energy (2.7 eV), environmental friendliness, and high stability in photocatalytic reactions, the photocatalytic activity of GCN has not yet met expectations in practical applications. To overcome this limitation, many studies have focused on enhancing the number of electron-hole pairs through structural modification, doping, and combination with other materials to create composite materials, providing favorable properties for the photocatalytic process.

1.4. Graphitic carbon nitride material (g-C_3N_4, GCN)

In Vietnam, many studies have employed semiconductor materials for the photocatalytic treatment of dyes and antibiotic residues. Among these materials, graphitic carbon nitride (GCN) has received considerable attention and is widely utilized in research. Most authors have focused on enhancing the photocatalytic performance of modified GCN through elemental doping and heterojunction engineering. The research group led by Vo Vien and colleagues at Quy Nhon University investigated the photocatalytic activity of modified GCN in combination with other materials. Specifically, Nguyen Van Phuc et al. successfully narrowed the bandgap of GCN by doping with oxygen and fluorine, achieving a photocatalytic degradation efficiency of 75% for Rhodamine B under visible light irradiation after 7 hours (Nguyen Van Phuc et al., 2019). However, the degradation efficiency remained relatively low and required a long reaction time. The team of Nguyen Thi Thanh Truc et al. demonstrated that the GCN/Cu-$NiWO_4$ composite achieved a photocatalytic degradation efficiency of 96.8% for n-hexane. Additionally, the Z-scheme heterojunction GCN/Cu-ZnO exhibited over 90% atrazine removal within 180 minutes, significantly outperforming either GCN or Cu-ZnO alone (Nguyen Thi Thanh Truc et al., 2019). Moreover, the composite material GCN/$CoFe_2O_4$/rGO was successfully synthesized via a

co-precipitation method and showed a tetracycline degradation efficiency of up to 95% after 240 minutes of reaction (Tram Pham Thi Le et al., 2022).

Globally, elemental doping and morphological engineering have proven to be effective strategies for enhancing the photocatalytic and electronic properties of graphitic carbon nitride (GCN). Elemental doping has been widely applied to modify GCN due to its relatively simple procedure and its significant impact on the electronic structure. Through doping, both the bandgap and the positions of the conduction band (CB) and valence band (VB) can be substantially altered. Moreover, even low concentrations of heteroatoms can significantly influence the charge distribution and physicochemical properties of GCN (Tian et al., 2017). Transition metals such as Zr, W, Cu, Fe, and Pd have been extensively used to modulate the electronic and optical behaviors of GCN. These dopants contribute to prolonging the charge carrier lifetime, accelerating charge mobility, narrowing the bandgap, and enhancing light absorption—factors that are crucial for improving photocatalytic performance. In addition, non-metallic elements such as halogens, boron, oxygen, nitrogen, carbon, sulfur, and phosphorus have been reported as effective dopants for GCN. While preserving its metal-free nature, non-metals often possess higher electronegativity and ionization energy, enabling them to form covalent bonds with GCN by accepting electrons. Furthermore, non-metal doping can also mitigate the effects of thermal fluctuations on chemical states (Lin, Hongxia, 2023). The electronic structure of GCN has also been successfully modified through sulfur doping, which enhances charge carrier mobility, redox ability, light absorption, and ultimately its photocatalytic activity (He et al., 2015). Modifying the morphology of GCN is another efficient approach to increasing its specific surface area and enhancing its photocatalytic activity. The primary morphologies of GCN include 0D (quantum dots), 1D (nanorods, nanowires, nanotubes), 2D (nanosheets), and 3D (porous frameworks) (Khan et al., 2020). Among these, 1D structures are particularly beneficial for promoting charge separation and facilitating photocatalytic reactions. The unidirectional structure of 1D GCN allows for axial electron

transport with minimal lateral scattering, offering a unique advantage in enhancing photocatalytic performance.

1.5. Key factors influencing photocatalytic performance

Effect of morphology and specific surface area

Photocatalytic reactions typically occur on the surface of semiconductor catalysts; therefore, the morphology and microstructural dimensions of the material are closely associated with its specific surface area and the number of accessible active sites, which can significantly influence its photocatalytic performance. Morphological engineering is thus considered a promising strategy for further enhancing the activity of GCN-based photocatalysts. GCN can be fabricated in a variety of morphological forms, including 0D (quantum dots), 1D (nanorods, nanowires, nanotubes), 2D (nanosheets), and 3D (porous structures) (Khan et al., 2020). Among these, 1D structures offer notable advantages due to their unidirectional framework, which facilitates the axial transport of photoinduced electrons while minimizing lateral scattering. This property greatly improves charge separation efficiency, which is crucial for accelerating photocatalytic reactions. Moreover, the physicochemical characteristics of 1D GCN can be finely tuned by adjusting the types of precursors, synthesis conditions, and other experimental parameters. Currently, common 1D GCN photocatalysts include nanofibers, nanowires, nanorods, and nanotubes.

Effect of pollutant concentration on photocatalytic efficiency

The concentration of pollutants plays a significant role in the generation of oxidative species such as hydroxyl radicals and superoxide radicals, which react with organic dyes like methylene blue (MB) and reactive black B (RBB). As the initial dye concentration increases, the likelihood of interactions between dye molecules and reactive radicals also increases, thereby accelerating the degradation rate. However, this effect has its limitations. At excessively high initial concentrations, the dye solution becomes increasingly turbid, which hinders photon penetration to the catalyst surface. As a result, more photons are absorbed or scattered by the dye molecules in solution instead of being utilized by the photocatalyst, ultimately reducing the degradation efficiency.

Nevertheless, doubling the concentration of both dye and catalyst up to 20 mg/L appeared to have minimal impact on conversion efficiency, especially for RBB, which exhibited negligible variation. Saquib and Muneer (2003) investigated the effect of organic compound concentration on the degradation of gentian violet at various concentrations (0.18, 0.25, 0.35, and 0.5 mM). Their results indicated that the degradation rate increased up to a concentration of 0.25 mM and then declined. Similarly, Kiriakidou et al. (1999) studied Acid Orange 7 (AO7) and obtained consistent findings. Their experiments, conducted at pH 6 and initial AO7 concentrations ranging from 25 to 600 mg/L, revealed that the time required for complete decolorization was strongly dependent on the initial dye concentration. Total decolorization was achieved in under one hour at relatively low concentrations (25–100 mg/L), whereas complete degradation did not occur at higher concentrations (200–600 mg/L).

Effect of catalyst concentration on photocatalytic efficiency

The concentration of the photocatalyst is a critical factor influencing the overall photocatalytic performance. It directly affects the number of active surface sites, light absorption capacity, and the extent of interaction between the catalyst and pollutants. An increase in catalyst dosage generally enhances the number of active sites available for the degradation process, thereby improving the removal efficiency of contaminants. However, excessive catalyst loading can lead to the aggregation of catalyst particles, which reduces the effective surface area and promotes light scattering rather than absorption. In such cases, the excessive turbidity of the suspension may hinder the penetration of light into the reaction medium, ultimately decreasing photocatalytic activity. Therefore, determining the optimal catalyst concentration is essential to maximize treatment efficiency while ensuring cost-effectiveness and material utilization.

Effect of ions on ohotocatalytic efficiency

Kumar et al. demonstrated that the degradation rate of chloramphenicol (CMP) increased with rising concentrations of CO_3^{2-} in deionized water when using a photocatalyst system of S@g-C_3N_4/B@g-C_3N_4, which is capable of generating $OH^{\bullet}$ under visible light irradiation. However, the overall removal of CMP was

inhibited in the presence of CO_3^{2-} due to the recombination of $OH^{\bullet}$ radicals. A similar inhibitory effect was observed for Ca^{2+} ions, which may form stable complexes with the pharmaceutical compound, thereby reducing its availability for photocatalytic degradation. When evaluating the photocatalytic efficiency of g-C_3N_4/$Bi_2O_2CO_3$ under solar irradiation for tetracycline (TC) degradation in real water matrices such as lake and well water, the degradation kinetics were found to be only slightly lower compared to those in deionized water. This minor reduction in performance could be attributed to the presence of various inorganic ions Cl^-, SO_4^{2-}, CO_3^{2-}, PO_4^{3-}, Fe^{3+}, Cu^{2+}, Ag^+, Ca^{2+}, Mg^{2+} and organic compounds in water.

Effect of pH on photocatalytic efficiency

pH is a key factor that directly influences the photocatalytic activity of a catalyst, primarily by altering its surface charge characteristics. The term "point of zero charge" (PZC) refers to the pH at which the net surface charge of the catalyst becomes zero. The zeta potential method is commonly employed to determine the surface charge behavior of photocatalytic materials. The initial pH of the dye solution also plays a significant role in determining the photocatalyst's effectiveness, as it affects the adsorption behavior and interfacial interactions. For instance, in a study investigating the pH-dependent degradation of methylene blue (MB) and reactive black B (RBB) in the pH range of 3 to 12, with fixed dye concentration (20 mg/L) and catalyst dosage (Fe/ZnO at 1 g/L), pH was shown to have a substantial influence on removal efficiency. The degradation efficiency increased markedly with rising pH, reaching a maximum at pH 9 for MB and pH 11 for RBB, and subsequently declined at higher pH values. The presence of H^+ ions was found to influence Zn^{2+} dissolution behavior. Under acidic conditions, the photocatalytic activity of Fe/ZnO declined, possibly due to photocorrosion and the acid-driven dissolution of ZnO. In contrast, under alkaline conditions, the catalyst exhibited enhanced performance—not only because of increased availability of hydroxyl ions (OH^-), but also due to suppression of ZnO dissolution. Notably, when the pH exceeded 9, no significant photocorrosion of Fe/ZnO was observed.

Reusability of the photocatalyst after multiple treatment cycles

To evaluate the stability of the g-C_3N_4/ZnS composite photocatalyst, repeated photocatalytic degradation experiments were conducted over several consecutive cycles. The composite material demonstrated nearly consistent photocatalytic performance throughout all five cycles. Nonetheless, a slight decline in activity (<5%) was observed, which may be attributed to inevitable losses of the photocatalyst during processes such as washing, centrifugation, sedimentation, and transfer. Additionally, this slight decrease in activity may be caused by morphological changes or redistribution of the ZnS component during the reaction process. Overall, the experimental results suggest that the g-C_3N_4/ZnS composite photocatalyst exhibits excellent stability and is well-suited for repeated use in practical photocatalytic applications (Ayodhya et al., 2019).

Effect of temperature on photocatalytic reactions

Temperature is a key parameter that influences photocatalytic processes, as it directly affects both the reaction rate and degradation efficiency of pollutants. With increasing temperature, molecules in the reaction system gain more thermal energy, which leads to a higher frequency of collisions between reactant molecules and catalyst particles, thereby accelerating the reaction kinetics. Furthermore, elevated temperatures increase the proportion of molecules with sufficient energy to overcome the activation barrier and participate in the reaction, ultimately improving the degradation efficiency. A review by Groeneveld et al. (2023) demonstrated the photocatalytic degradation performance of rhodamine B at different temperatures using Ag-doped TiO_2 particles and Ag-doped TiO_2 nanofibers, confirming that temperature plays a significant role in enhancing photocatalytic activity.

Chapter 2. OBJECTIVES, SCOPE, CONTENT, AND RESEARCH METHODS

2.1. Objectives, scope, location, and duration

2.1.1. Research objectives

- Undoped graphitic carbon nitride (GCN) nanomaterial and boron (B) doped GCN material with a hollow tubular shape (1D).
- Antibiotic residues simulated under laboratory conditions (SMX, TC, DCF, CIP).

2.1.2. Scope of Research

- The research was conducted under laboratory conditions on a small scale to evaluate the ability and efficiency of the material in treating antibiotic residues.

2.1.3. Research Location CRRC

- Laboratory at the Center of crop research for adaptation to climate change, University of Agriculture and Forestry - Thai Nguyen University.
- Physics, Chemistry, and Biomedical Laboratory, Faculty of Basic Sciences, University of Medicine and Pharmacy - Thai Nguyen University.

2.1.4. Research Duration

- From 2020 to 2024.

2.2. Research Content

The research content is summarized by the author in Figure 2.1, which describes the synthesis process of 1D B-doped GCN nanomaterial and its application in treating some antibiotic residues in water environments, including:

Content 1: Fabrication of boron (B)-doped GCN nanomaterial with a tubular structure using (1) the direct thermal polymerization method (1DBCN); (2) the hydrolysis and high-temperature thermal polymerization method (TGCN-Bx). Evaluation of the basic characteristics of the material such as crystal structure, morphology, surface area, chemical composition, optical properties, band gap energy, and electron-hole recombination ability of the material through modern techniques such as TEM, SEM, EDS, XRD, BET, FTIR, XPS, DRS, EIS…

Content 2: Research on the application of B-doped GCN material using photocatalytic technology in the treatment of antibiotic residues. Investigation of several factors affecting the degradation efficiency of antibiotic residues by the B-doped GCN material, such

as pollutant concentration, pH value, the influence of interfering ions, and the reusability of the material after 5 treatment cycles.
Content 3: Proposal of the treatment mechanism for antibiotic residues by the B-doped GCN material.

2.3. Chemicals and equipment

2.4. Research methods

2.4.1. Methods for material fabrication

2.4.1.1. Fabrication of tubular B-doped GCN nanomaterial by direct thermal polymerization

In this study, tubular B-doped GCN nanomaterial was fabricated using a modified direct thermal polymerization method based on the research of Liu et al. (2021). The synthesis method involved 3 steps, with the experimental steps in the following order:

Step 1: Preparation of the material mixture: Accurately weigh the materials Melamine, Urea, and Boric acid according to the following mass ratio: 1:10:0.1. Mix thoroughly and grind the chemicals into a fine powder in an agate mortar. Transfer the mixed mixture into a covered crucible and seal it with aluminum foil.

Step 2: Thermal Polymerization Process: Place the crucible in a limited-oxygen furnace. Set the furnace program as follows: Target temperature: 600°C; heating time: 4 hours; heating rate: 10°C/minute.

Step 3: Sample Recovery and Storage: After the furnace returns to room temperature, remove the crucible. Recover the sample and transfer the powder sample into a sealed tube. The tubular B-doped GCN nanomaterial sample is labeled as 1DBCN, which is yellow and in the form of a porous powder. The flowchart of the fabrication process of tubular B-doped GCN nanomaterial is shown in Figure 2.2.

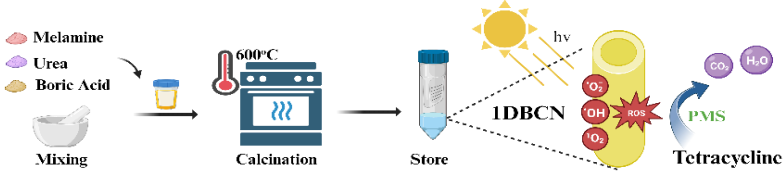

Figure 2.2. Flowchart of the 1DBCN material fabrication process

Control materials:

The 2D GCN nanosheet material was synthesized via direct thermal polymerization. The precursors used were melamine and urea in a weight ratio of 1:1, without the addition of boric acid. The mixture was placed into a crucible and transferred into a muffle furnace under limited oxygen conditions. The thermal treatment was carried out at 600°C for 4 hours with a heating rate of 10°C/min. After completion, the material was allowed to cool naturally. The resulting yellow powder was stored in a sealed tube. The obtained sample was designated as 2DGCN.

The 1D tubular GCN material was also synthesized via direct thermal polymerization. The melamine and urea precursors were mixed in a weight ratio of 1:10, without the use of boric acid. The mixture was placed into a crucible and transferred into a muffle furnace under limited oxygen conditions. The thermal treatment was performed at 600°C for 4 hours with a heating rate of 10°C/min. Upon completion, the material was naturally cooled. The resulting yellow powder was stored in a sealed tube. The obtained sample was designated as 1DGCN.

2.4.1.2. Fabrication of tubular B-doped GCN nanomaterial by hydrolysis and high-temperature thermal polymerization

In this study, the tubular boron-doped graphitic carbon nitride (B-doped GCN) nanomaterial was synthesized using a modified direct thermal polymerization method based on the work of Niu et al. (2021). Specifically, the synthesis of 1D tubular B-doped GCN was carried out through a combination of hydrothermal treatment and thermal polymerization, involving the following five steps: Step 1: Preparation of Solution A Accurately weigh 0.01 mol of cyanuric acid and varying amounts of H_3BO_3 (0.125, 0.25, 0.5, or 1 mmol), and add them to a glass beaker containing 50 mL of deionized water. Place the beaker on a hotplate, heat the solution to 90°C, and stir until all components are fully dissolved. Step 2: Preparation of Solution B Accurately weigh 0.01 mol of melamine and add it to a separate glass beaker containing 50 mL of deionized water. Heat the

solution to 90°C on a hotplate and stir until completely dissolved. Step 3: Mixing and Hydrothermal Reaction Slowly add Solution B to Solution A to form a suspension containing supramolecular intermediates. Transfer the mixture into a round-bottom flask equipped with a reflux condenser. Adjust the cooling water flow to maintain proper condensation temperature. Heat the mixture to 120°C and stir vigorously for 12 hours. Step 4: Drying the Sample Transfer the resulting suspension from the flask into a glass dish. Dry the mixture overnight at 60°C. Step 5: Calcination and Product Collection Place the dried white solid into a sealed crucible. Calcine the sample at 600°C for 4 hours in a muffle furnace under limited oxygen, with a heating rate of 2°C/min. After the furnace cools to room temperature, collect the material and store it in a sealed vial. The final product is denoted as TGCN-Bx, where 'x' corresponds to the molar amount of H_3BO_3 used (0.125, 0.25, 0.5, or 1 mmol). The synthesis process is illustrated in Figure 2.3.

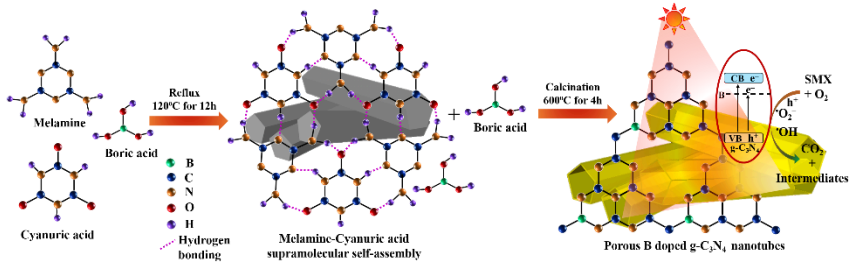

Figure 2.3. Flowchart of the TGCN-Bx material fabrication process

Control Material:

The 1D tubular GCN nanomaterial without boron doping was synthesized via a combination of hydrothermal treatment and thermal polymerization. Cyanuric acid was dissolved in deionized water to form a solution. Similarly, melamine was dissolved separately to prepare a second solution. The two solutions were then thoroughly mixed and transferred into a round-bottom flask. The reaction mixture was heated at 120°C for 12 hours to form a suspension. The suspension was subsequently dried at 60°C and finally calcined at

600°C for 4 hours to obtain the final product. The resulting material was denoted as TGCN.

In summary, boron-doped GCN materials were synthesized using two different methods, as described in Tables 2.2 and 2.3.

Table 2.2. Sample codes of boron-doped GCN synthesized via direct thermal polymerization method

No.	Material Name	Sample Symbol	Precursor	Synthesis method
1	Graphitic Carbon Nitride (Sheet form, non-doped)	Mẫu đối chứng 2DGCN	Melamine, Urea (wt%:wt% = 1:1)	Thermal decomposition: 600°C, 4 hours
2	Graphitic Carbon Nitride (Tube form, non-doped)	1DGCN	Melamine, Urea (wt%:wt% = 1:10)	Thermal decomposition: 600°C, 4 hours
3	Graphitic Carbon Nitride (Tube form, doped with B)	1DBCN	Melamine, Urea, H_3BO_3 (wt%:wt%:wt% = 1:10:0.1)	Thermal decomposition: 600°C, 4 hours

Table 2.3. Sample codes of boron-doped GCN synthesized via a combination of hydrothermal treatment and direct thermal polymerization

No.	Material Name	Sample Symbol	Precursor	Synthesis Method
1	Graphitic Carbon Nitride (Tube form, non-doped)	Control Sample TGCN	Cyanuric Acid, Melamine (mol = 0.01:0.01)	Hydrolysis: 120°C, 12 hours; Thermal decomposition: 600°C, 4 hours
2	Graphitic Carbon Nitride (Tube form, doped with B)	TGCN-Bx (x = 1 to 4, corresponding to H_3BO_3 additions of 0.125, 0.25, 0.5, 1 mmol)	Cyanuric Acid, Melamine (mol = 0.01:0.01); H_3BO_3 = 0.125, 0.25, 0.5, 1 mmol	Hydrolysis: 120°C, 12 hours; Thermal decomposition: 600°C, 4 hours

2.4.2. Methods for characterizing the properties of research materials

The physicochemical properties of the materials, including morphology, crystallinity, specific surface area, pore size distribution, and surface chemical species of the GCN and doped GCN materials, are characterized by SEM, TEM, XRD, BET, XPS, FTIR, and DRS. The electrochemical properties are obtained using the electrochemical testing system Autolab PGSTAT 302N (Metrohm Autolab B.V., Netherlands) with NOVA software.

2.4.3. Pollutant quantification method

2.4.4. Evaluation of antibiotic residue removal in water using photocatalytic technology with doped GCN materials

Initially, a specified amount of photocatalyst (0.25–1 g/L) was added to a pollutant solution with a concentration ranging from 5 to 40 mg/L and an adjusted pH between 3 and 11. The mixture was then thoroughly stirred in double-jacketed reaction vessels equipped with a circulating water system to maintain the reaction temperature at 25°C. The suspension was kept in the dark for 30 minutes while being stirred at 4000 rpm to achieve adsorption–desorption equilibrium. Subsequently, photocatalytic degradation was initiated by irradiating the suspension with a xenon lamp. If required, a peroxymonosulfate (PMS) solution (0.3 mM) was added at this stage. At predetermined time intervals, aliquots were withdrawn and analyzed for pollutant concentration using either a UV-Vis spectrophotometer or UPLC. The procedure was repeated over time to monitor the degradation kinetics. Each experiment was conducted in triplicate to ensure the reliability and reproducibility of the results.

Chapter 3. RESULTS AND DISCUSSION

3.1. Tubular B doped GCN material synthesis via Direct Thermal Decomposition (1DBCN) and Its Photocatalytic Application

3.1.1. Physicochemical properties of 2DGCN, 1DGCN, and 1DBCN materials

The morphology of 2DGCN in sheet form is shown in Figure 3.1 (a), while the tubular material shown in Figure 3.1 (b) is derived from 1D tubular material. The difference in morphology may be due to the mass ratio difference between melamine and urea. With a mass ratio of 1:1, melamine and urea molecules are arranged more randomly in the two-dimensional (2D) sheets, resulting in a thicker, uneven structure. However, a mass ratio of 1:10 between melamine and urea leads to the formation of 1D nano-tubes with a length of about 3 µm and a diameter of 300 nm. The incorporation of boron (B) into GCN maintains the hollow structure with open ends, as observed in the SEM images (Figures 3.1 (c) and (d)). This unique shape and structure allow for a large surface area, providing an excellent foundation for catalytic and chemical reactions.

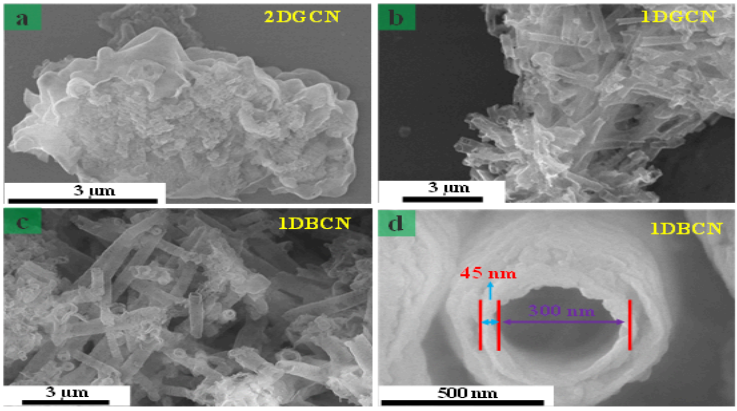

Figure 3.1. SEM images of (a) 2DGCN, (b) 1DGCN, (c) and (d) 1DBCN nano-tubes

The crystalline properties and chemical composition of the materials were further analyzed using X-ray diffraction (XRD) and Fourier-transform infrared (FTIR) spectroscopy. All samples exhibited two characteristic diffraction peaks associated with

graphitic carbon nitride (GCN), located at approximately 13.1° and 27.3°. In addition, FTIR spectroscopy was employed to elucidate the structural and chemical features of GCN. The characteristic FTIR signals corresponding to tri-s-triazine units (810 cm^{-1}), nitrogen-containing aromatic heterocycles (1200–1700 cm^{-1}), and the stretching vibrations of non-condensed amino groups (N–H) in the range of 3000–3500 cm^{-1} were simultaneously identified (Huang et al., 2023). The estimated bandgap energies (E_g) of the 1BDCN and 1DGCN samples were approximately 2.7 eV and 2.8 eV, respectively, which are slightly lower than that of bulk 2DGCN (2.82 eV). The incorporation of boron into 1BDCN resulted in a mild reduction in the bandgap, potentially due to the introduction of mid-gap states.

3.1.3. Photocatalytic degradation of TC using materials with PMS assistance

When using PMS and light without a photocatalyst, the TC removal rate is relatively low, with less than 20% of TC removed. These results indicate that the effectiveness of visible light and PMS alone in removing TC is limited. However, when a photocatalyst is added with the presence of 0.3 mM PMS, a significant increase in TC degradation is observed under visible light. Notably, the conversion of 2D nanosheets into 1D nanotubes has been shown to be beneficial for TC degradation. The 1DGCN nanotubes exhibited a much higher TC degradation performance, achieving 82%, compared to the 55% degradation achieved by the 2DGCN sample. Remarkably, 1DBCN exhibited an enhanced TC removal efficiency of up to 99%, showing that PMS activation with light irradiation effectively promotes the oxidation process of TC. The improved performance of TC degradation when using photocatalytic materials with the support of light and PMS is due to the optimal combination of several factors. First, 1DBCN has the largest specific surface area (81.1 m^2/g) compared to 1DGCN (56.56 m^2/g) and 2DGCN (35.4 m^2/g), and the lowest band gap energy (2.7 eV) compared to 1DGCN and 2DGCN. The specific surface area of 1DBCN is approximately 1.4 times greater than 1DGCN and 2.3 times greater than 2DGCN, providing more active sites for photocatalytic processes when PMS

is activated to generate ROS, thus enhancing the degradation of TC molecules.

For 1DBCN, the calculated rate constant (k) is 0.078 min^{-1}, showing a degradation rate that is approximately 1.56 times faster than 1DGCN (k = 0.05 min^{-1}) and about 2.8 times faster than 2DGCN sheets (k = 0.027 min^{-1}). This comparison highlights the superior performance of 1DBCN in the rate of TC degradation. Another experiment was conducted to examine the effect of the initial PMS concentration on TC degradation (Figure 3.4 (b)). The results show that after 30 minutes, TC removal rates of 17%, 80%, and 99% were achieved with PMS concentrations ranging from 0.1 mM to 0.3 mM. The rate constant for 0.3 mM PMS was determined to be 0.078 min^{-1}, which is higher than the rate constants for 0.2 mM PMS (0.026 min^{-1}) and significantly higher than for 0.1 mM PMS (0.007 min^{-1}).

Table 3.1. Comparison of the characteristics of nano materials 2DGCN, 1DGCN, and 1DBCN

Material	Morphology	Bandgap (eV)	Surface Area (m^2/g)	Efficiency (%)	Rate Constant (k) (min^{-1})
2DGCN	Sheet (2D)	2.82	35.4	55	0.027
1DGCN	1D	2.8	56.56	82	0.05
1DBCN	1D	2.7	81.1	99	0.078

3.1.4. Study on the reusability of 1DBCN material and photocatalytic performance in SMX, CIP degradation

The photocatalyst exhibited a high level of reusability during tetracycline (TC) degradation, maintaining 82% removal efficiency after five treatment cycles. The fact that the material's performance decreased by only 10% after repeated use indicates excellent structural stability. Its resistance to chemical agents and oxidative conditions enables the photocatalyst to retain its original properties throughout the treatment process. This durability is not only economically advantageous but also highly beneficial for the long-term sustainability of wastewater treatment systems. High reusability significantly reduces operational costs, minimizes the frequency of material replacement, lowers waste generation, and decreases the demand for new material synthesis, thereby

contributing to environmental protection. The excellent stability of the material makes it a promising candidate for implementation in large-scale wastewater treatment systems, offering advantages in reduced maintenance time and operational cost.

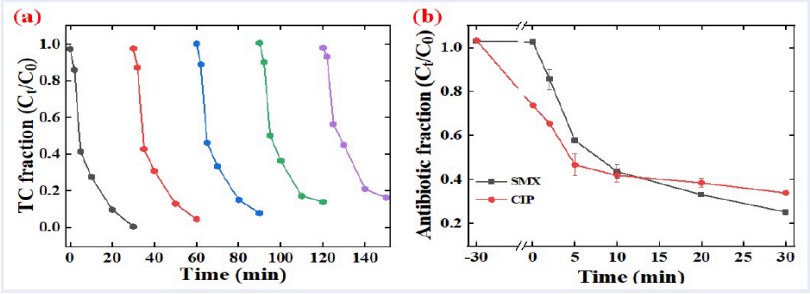

Figure 3.7. (a) Reusability of 1DBCN material after 5 cycles of TC degradation and (b) 1DBCN material performance in degrading SMX and CIP.

3.2. Synthesized tubular B-doped GCN material via hydrolysis and thermal decomposition (TGCN-Bx) and photocatalytic application

3.2.1. Physicochemical properties of TGCN and TGCN-Bx

The tubular structure of g-C_3N_4 gradually evolved from a solid 1D rod-like morphology with a diameter ranging from 0.5 to 1 micrometer (Jourshabani et al., 2022; Weers et al., 2023). In the subsequent step, the white solid was heated at 60 °C to facilitate evaporation, followed by calcination at 600 °C under limited oxygen conditions. During this thermal process, the solid rod-like 1D structure was transformed into a hollow tubular form, featuring multiple surface pores and open ends at both extremities.

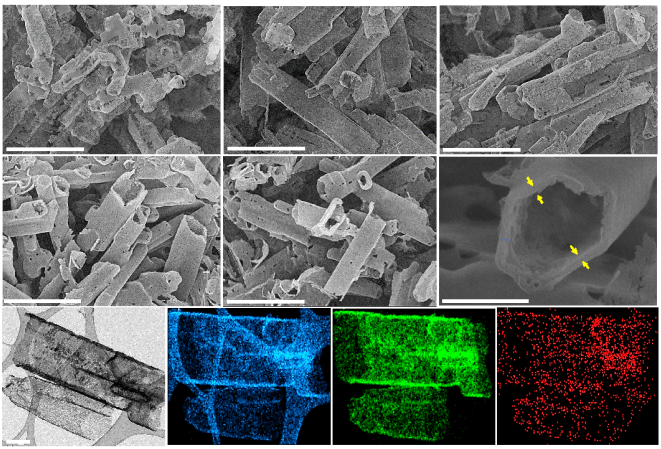

Figure 3.9. SEM images of (a) TGCN, (b) TGCN-B1, (c) TGCN-B2, (d) TGCN-B3, (e) TGCN-B4, (f) TGCN-B2, (g) TEM image of TGCN-B2, (h) Elemental mapping of carbon (C), nitrogen (N), boron (B) and EDS spectrum of TGCN-B2

This structural transformation contributed to a significant increase in the specific surface area of TGCN-Bx (ranging from 85 to 98 m^2/g) compared to that of TGCN (56 m^2/g), which is favorable for enhancing photocatalytic activity. The X-ray diffraction (XRD) pattern of TGCN exhibited two characteristic peaks at $2\theta = 13.5°$ and 27.5°, corresponding to the (100) and (002) crystal planes of GCN, respectively. The FTIR spectra displayed vibrational bands in the range of 808 and 900–1800 cm^{-1}, which are assigned to the typical bending modes of triazine units and N–C=N/N–C_3 heterocyclic rings within the framework. Additionally, bands observed between 3010 and 3500 cm^{-1} were attributed to the stretching vibrations of NH_2/N–H groups, indicating that the GCN obtained via direct thermal treatment was not fully condensed and that N–H bonds remain at the edges of the layered structure. However, the in-plane B–N vibrations were typically undetectable due to their overlap with the stretching bands of C–N (Preeyanghaa et al., 2022). The estimated bandgap energies of TGCN and TGCN-Bx (x = 1, 2, 3, 4) were 2.70, 2.68, 2.66, 2.64, and 2.61 eV, respectively, demonstrating

an increasing trend in visible light absorption capability with increasing boric acid dosage.

3.2.3. Photocatalytic degradation of SMX using TGCN and TGCN-Bx materials

Selection of the optimal photocatalyst for SMX degradation

TGCN-Bx photocatalysts exhibited higher photocatalytic activity for sulfamethoxazole (SMX) degradation compared to undoped TGCN. However, an increase in boron content beyond the optimal level resulted in a slight reduction in photocatalytic efficiency. After 30 minutes of visible light irradiation, the SMX removal efficiencies of TGCN-B1, TGCN-B2, TGCN-B3, TGCN-B4, and TGCN were found to be 95%, 99%, 98%, 93%, and 68%, respectively. Notably, TGCN-B2, which was synthesized with 0.25 mmol of boric acid, achieved the highest SMX degradation efficiency at 99%. The corresponding apparent rate constants (k) for SMX degradation by TGCN, TGCN-B1, TGCN-B2, TGCN-B3, and TGCN-B4 were 0.038, 0.093, 0.201, 0.0128, and 0.074 min^{-1}, respectively. Remarkably, the rate constant of TGCN-B2 was approximately 5.2 times higher than that of undoped TGCN, confirming its superior photocatalytic performance.

Table 3.2. Comparison of TGCN and TGCN-BX material properties

Material	Band Gap Energy (eV)	Surface Area (m^2/g)	Removal Efficiency (%)	Reaction Rate (min^{-1})
TGCN	2.7	56	68	0.038
TGCN-B1	2.68	91	95	0.093
TGCN-B2	2.66	98	99	0.201
TGCN-B3	2.64	90	98	0.0128
TGCN-B4	2.61	85	93	0.074

Optimization of reaction parameters: Catalyst Dosage, initial SMX concentration, pH, and water matrix effects

The photocatalytic efficiency of the catalyst is typically influenced by various environmental parameters, including catalyst dosage, initial pollutant concentration, pH, and the presence of interfering substances within the water matrix. The results demonstrated that increasing the catalyst dosage from 0.25 g/L to 1.0 g/L significantly enhanced the SMX degradation efficiency, reaching

a maximum of 99% after 30 minutes at 1.0 g/L. Specifically, at 0.25 g/L, the degradation efficiency was only around 60% after 30 minutes, while it increased to 80% at 0.50 g/L and further to 90% at 0.75 g/L. These findings indicate that increasing catalyst dosage improves SMX degradation efficiency, particularly when reaching 1.0 g/L. In contrast, a notable decrease in degradation efficiency—from 99% to 40%—was observed when the initial SMX concentration was increased from 5 to 40 mg/L. This finding highlights the strong influence of pollutant concentration on photocatalytic performance. At higher SMX concentrations, the TGCN-B2 photocatalyst became saturated with SMX molecules, thereby limiting active site availability and reducing degradation efficiency.

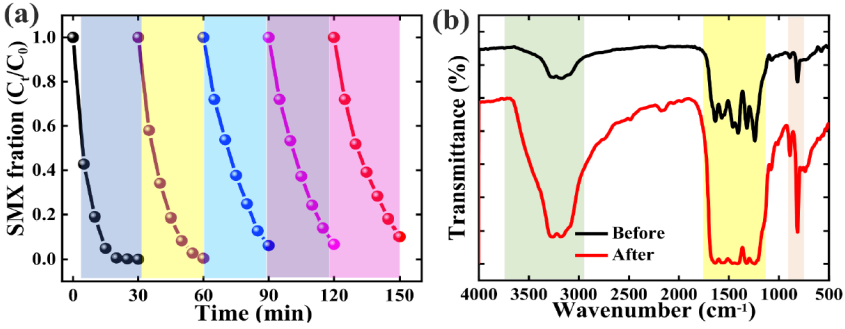

Figure 3.21. (a) Reusability of 5 cycles and (b) FTIR before and after photodegradation reaction

3.3. Proposed mechanism for antibiotic degradation using 1DBCN and TGCN-Bx under visible light irradiation

Based on the experimental findings, a plausible reaction mechanism is proposed for the PMS-assisted synergistic photocatalytic system (Figure 3.23). Upon exposure to visible light, photoexcited electrons (e^-) and holes (h^+) are generated. The photogenerated e^- in the conduction band (CB) of 1DBCN can reduce molecular oxygen (O_2) to generate superoxide anion radicals ($O_2^{\bullet-}$) ($O_2 \rightarrow O_2^{\bullet-}$, E_H = -0.33 eV versus NHE) (Bai, Xue et al., 2023). Simultaneously, in the presence of peroxymonosulfate (PMS),

the e^- can reduce PMS to generate sulfate radicals ($SO_4^{\bullet-}$), while h^+ can oxidize HSO_5^- to form peroxymonosulfate radicals ($SO_5^{\bullet-}$), as described in Equations (3) and (4). The formation of singlet oxygen ($^1O_2$) can proceed via multiple pathways involving SO_5^- or $O_2^{\bullet-}$ intermediates, as indicated in Equations (5), (6), and (7) (Jing et al., 2023). Ultimately, the active species h^+, $^\bullet OH$, $SO_4^{\bullet-}$, $O_2^{\bullet-}$, and $^1O_2$ synergistically contribute to the efficient degradation of tetracycline (TC) in the photocatalytic system.

$$\text{Catalyst} + h\nu \rightarrow h^+ + e^- \quad (1)$$

$$e^- + O_2 \rightarrow O_2^{\bullet-} \quad (2)$$

$$HSO_5^- + e^- \rightarrow SO_4^{\bullet-} + OH^- \quad (3)$$

$$HSO_5^- + h^+ \rightarrow SO_5^{\bullet-} + OH^- \quad (4)$$

$$2SO_5^{\bullet-} \rightarrow 2SO_4^{\bullet-} + {}^1O_2 \quad (5)$$

$$SO_4^{\bullet-} + OH^- \rightarrow SO_4^{2-} + {}^\bullet OH \quad (6)$$

$$^\bullet O_2^- + 2H_2O \rightarrow {}^1O_2 + H_2O_2 + 2H^+ \quad (7)$$

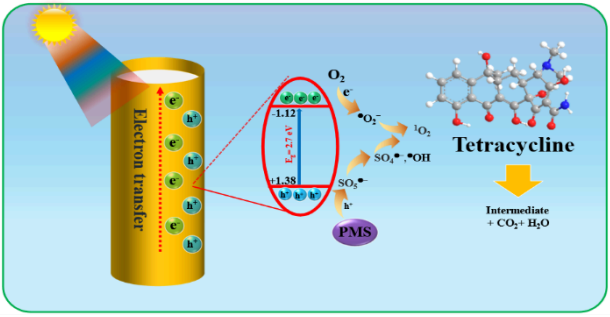

Figure 3.23. The possible mechanism for TC photodegradation over 1DBCN for PMS activation under visible light irradiation

Quenching experiments were performed with different scavengers to evaluate the role of the different active species in SMX degradation using TGCN-B2 under visible light. The decrease in SMX concentration over time was observed with different quenchers. In particular, methanol (Met), ascorbic acid (AA), and ethylenediaminetetraacetic acid tetrasodium salt dehydrate (EDTA.2Na) were used to identify the presence of $^\bullet OH$, $O_2^{\bullet-}$, and h^+ in the reaction, respectively, as quenching agents. After 30 minutes

of reaction, the photocatalytic removal efficiency of SMX on TGCN-B2 was determined to be 39%, 8%, and 97% with the presence of AA, EDTA.2Na, and Met. The results indicated that both $O_2^{\bullet-}$ and h^+ are the primary species which is responsible for the degradation of SMX.

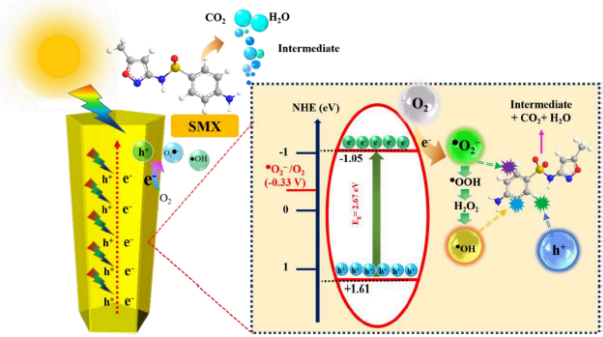

Figure 3.25. Schematic illustration of the photocatalytic degradation of SMX utilizing TGCN-B2 catalyst under visible light irradiation

The photocatalytic degradation mechanism can be summarized as follows:

$TGCN\text{-}B2 + hv \rightarrow h^+_{VB} + e^-_{CB}$ (1)

$e^-_{CB} + O_2 \rightarrow O_2^{\bullet-}$ (2)

$O_2^{\bullet-} + H^+ \rightarrow {}^{\bullet}OOH$ (3)

$e^-_{CB} + {}^{\bullet}OOH + H^+ \rightarrow H_2O_2$ (4)

$e^-_{CB} + H_2O_2 \rightarrow OH^{\bullet} + OH^-$ (5)

$SMX + ROS\ (O_2^{\bullet-}, h^+, OH^{\bullet}) \rightarrow Intermediate + CO_2 + H_2O$ (6)

3.4. Comparison and evaluation of 1DBCN and TGCN-B2 materials

In the comparative study on pollutant removal efficiency, TGCN-B2 that synthesized via a two-step hydrothermal and thermal polymerization process was demonstrated superior degradation performance compared to 1DBCN, which was prepared via direct thermal polymerization. This difference can be attributed to structural factors such as the larger surface area, greater pore volume

and size, and more efficient boron doping in TGCN-B2, all of which contributed to enhanced photocatalytic performance.

Table 3.4. Comparison of photocatalytic performance for antibiotic residue degradation using 1DBCN and TGCN-B2

Reaction Conditions	Removal efficiency under visible light irradiation			
Pollutant Material	TC	SMX	CIP	DCF
1DBCN	2%	5%	7%	12%
TGCN-B2	25%	99%	3%	87%
	Removal Efficiency Under Visible Light and the Presence of PMS			
1DBCN	99%	76%	61%	94%
TGCN-B2	99%	99%	96%	99%

CONCLUSION AND RECOMMENDATIONS

1. Conclusion

- In this study, boron-doped graphitic carbon nitride (g-C_3N_4) nanomaterials were successfully synthesized using two different fabrication methods: direct thermal polymerization (1DBCN) and a combined hydrothermal and high-temperature thermal polymerization method (TGCN-Bx). Both methods produced hollow nanotube structures upon calcination at 550–600°C. After boron doping, the morphology of the materials did not change significantly compared to pristine g-C_3N_4. Specifically, 1DBCN exhibited a uniform tubular structure with dimensions of approximately 3 × 300 nm and a specific surface area of 81.1 m²/g, while TGCN-Bx presented more diverse morphology and higher surface areas ranging from 85 to 98 m²/g, indicating enhanced application potential. The bandgap energy of the materials was notably reduced after boron doping, with an optimal boron content of 2.41 wt%.

- The 1DBCN photocatalyst, in combination with PMS and visible light, achieved up to 99% removal of tetracycline (TC), which was 5.2 times higher than that of undoped g-C_3N_4, under optimal conditions of 0.5 g/L catalyst dosage, pH 7, and 0.3 mM PMS. Meanwhile, TGCN-B2 achieved its highest SMX removal efficiency

at a catalyst concentration of 1 g/L, SMX = 10 mg/L, and pH = 7, while also demonstrating good reusability with a maintained degradation efficiency above 82% after five cycles. Despite slight environmental interferences, TGCN-B2 maintained degradation performance above 80%. Comparative evaluation confirmed that TGCN-B2, synthesized via the hydrothermal–thermal two-step method, exhibited significantly superior pollutant removal performance compared to 1DBCN, which was synthesized via direct thermal polymerization.

- Radical scavenging experiments and electron paramagnetic resonance (EPR) analysis confirmed the generation of multiple reactive species, including $O_2^{\bullet -}$, •OH, h^+, $^1O_2$, and $SO_4^{\bullet -}$, on the surface of 1DBCN under PMS activation and light irradiation. Similarly, TGCN-B2 predominantly generated $O_2^{\bullet -}$, h^+, and •OH radicals. These reactive species played critical roles in the effective degradation of organic pollutants.

2. Recommendations

- To further expand the applicability of tubular boron-doped g-C_3N_4 nanomaterials, in-depth studies should focus on the degradation of other complex organic pollutants such as pesticides, dyes, and persistent organic compounds. Moreover, applying this material to the treatment of actual wastewater, particularly from industrial and urban sources, and conducting pilot- and field-scale operations will provide a more comprehensive assessment of its performance and competitiveness compared to existing technologies.

- The photocatalytic process may be further enhanced through integration with other treatment technologies such as adsorption, biological treatment, or membrane filtration. Additionally, optimizing reaction conditions, elucidating the reaction mechanisms, and scaling up material synthesis are critical directions for future research and development.